26 May 2010, 4:45 pm - 6:45 pm

Centrifuge Modeling of the Influence of Pre-Existing Fractures in Multilayered Soils on Ground Deformations

P. Hu
Beijing Seismological Bureau, Beijing, China

Y. H. Ding
Beijing Seismological Bureau, Beijing, China

Q. P. Cai
Hong Kong University of Science and Technology, Hong Kong

G. Y. Luo
Hong Kong University of Science and Technology, Hong Kong

C. W. W. Ng
Hong Kong University of Science and Technology, Hong Kong


Fifth International Conference on
Recent Advances in Geotechnical Earthquake Engineering and Soil Dynamics
and Symposium in Honor of Professor I.M. Idriss
May 24-29, 2010 • San Diego, California

CENTRIFUGE MODELING OF THE INFLUENCE OF PRE-EXISTING FRACTURES IN MULTILAYERED SOILS ON GROUND DEFORMATIONS

P. Hu, Y. H. Ding
Beijing Seismological Bureau
No. 28, SuZhou Street, Beijing, China 100080

Q. P. Cai, G. Y. Luo, C. W. W. Ng, Y. J. Hou
Hong Kong University of Science and Technology
Clear Water Bay, Kowloon, HKSAR

ABSTRACT

Fault rupture propagation in free fields lays the ground for an understanding of bedrock-soil-structure interactions. Propagation behaviors in dry soil have long been investigated. Localized shear bands have been identified to be the obvious source of failure in dry soils at depth. In addition, numerous subsurface fractures have been found in the field. However, the influence of subsurface fractures in the soil on future seismic faults has received little attention, especially in complex soils. In this study, three centrifuge tests were conducted to investigate the influence of pre-existing fractures on ground deformations in three multilayered soils: three-layered, five-layered and nine-layered soils. The pre-existing fractures in these tests started from the bedrock fault line and tilted with a dip slip angle of 70^o with respect to the horizontal plane. In this paper, both of the ground surface settlement and the bedrock fault movements are presented. Post test examination of the cracks on model surface are also described and compared to studies that did not consider the influence of pre-existing fractures.

INTRODUCTION

There is no doubt that many buildings are located in potentially dangerous areas that are subjected to bedrock fault movements. Engineers responsible for the design and construction of these buildings must possess skills and techniques to estimate potential ground movements to be able to assess whether or not these buildings can withstand excessive differential settlements or severe foundation distortion if an earthquake occurs.

Ground failure induced by bedrock fault movements is now a cause for increasing concern (Anastasopoulos et al. 2009; Ahmed and Bransby 2009). In previous studies, the bedrock-soil-structure interaction during normal fault and reverse fault movements was investigated. A nonlinear finite-element model was built to study rupture propagation and its interaction with strip foundations. This methodology was validated through class "A" predictions of centrifuge model tests and was then applied to a series of parameter studies. Even though important knowledge on the interaction behavior was obtained in these studies, free field test results provide the necessary groundwork for understanding more complex cases.

From field observations and physical model tests (Cole and Lade 1984; Bray et al. 1994; Lazarte and Bray 1996), it has long been recognized that "ductility" is a crucial influencing factor in the fault rupture propagation problem. Less bedrock fault movement is required to propagate a shear rupture to the ground surface through a layer of relatively brittle material than through a ductile material. Ductile materials can accommodate significant bedrock fault movements without the scarping of the ground surface that may occur in brittle materials. Numerical analysis also reveals the importance of appropriate soil models (Athanasopoulos 2009; Anastasopoulos 2009). Inappropriate soil information may result in unrealistic and even misleading test results.

Physical model tests showed that localized shear failure was the most severe failure pattern occurring in dry particulate soil at depth (Cole and Lade 1984). In real soil, there are also numerous subsurface fractures left behind by previous seismic activity. There is no doubt that these subsurface fractures may also influence fault rupture propagation during future seismic activities (Bray et al. 1994; Faccenna et al. 1995). Lade et al. (1984) conducted sandbox tests to investigate the multiple failure surfaces that may be triggered by reversing the direction of the bedrock fault movement after a normal fault. By comparing the test results with field case studies, they concluded that the influence of an existing failure surface on the location of subsequent failure surfaces developed by reversing the direction of movement is small to negligible. But it is apparent that the dry sand material adopted in the tests restricts the application of their conclusion.

Hu et al. (2009) reported a centrifuge test on a nine-layered soil model to investigate ground failure induced by a normal fault. Surface cracks on the ground were found to be a major failure pattern that may be induced by normal fault movements in nine-layered soil. This failure pattern can also be observed in silt. In the present study, ground deformations of three-layered, five-layered and nine-layered soil samples subjected to normal faults were investigated using centrifuge tests. The influence of pre-existing fractures on ground deformation was also investigated in this study

CENTRIFUGE MODEL TESTING

Test Program

The experimental program was designed to evaluate the influence of pre-existing fractures on ground failures induced by normal fault movements. Three centrifuge tests were conducted in the 400 g-ton, 8.5 m diameter geotechnical beam centrifuge at the Hong Kong University of Science and Technology, which is equipped a hydraulic bi-axial shaking table (Ng et al. 2001; Ng et al. 2004). Figure 1(a) shows the geometries of the three-layered model with a pre-existing fracture in test 3LuR. This pre-existing fracture started from the bedrock fault line and tilted with a targeted angle of with respect to the horizontal plane. The height of the pre-existing fracture was 437mm.

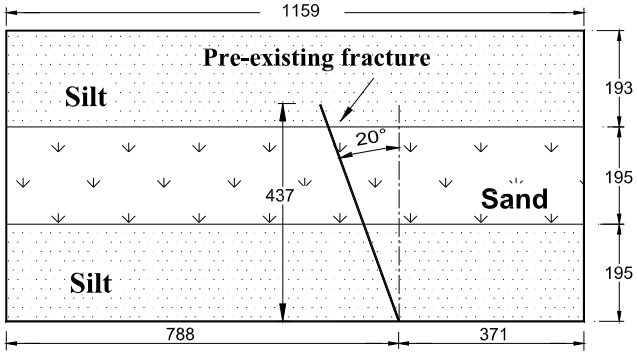

(a) Test 3LuR

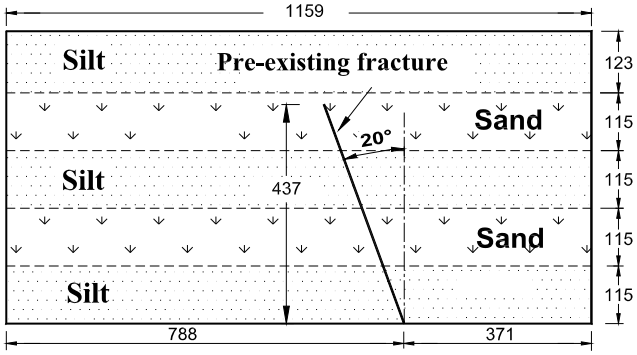

(b) Test 5LuR

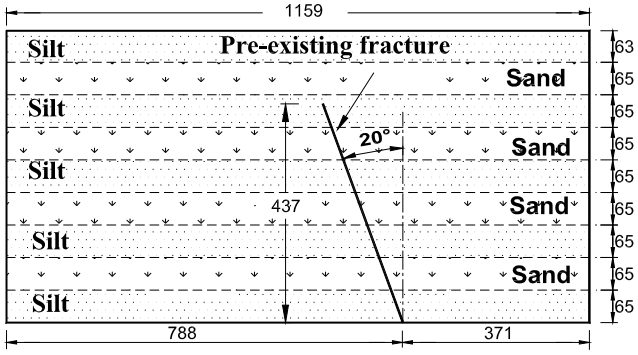

(c) Test 9LuR$^+$

Fig. 1. Schematic diagram of the soil models (dimensions in mm).

Figures 1(b) and 1(c) show the five-layered model in test 5LuR and the nine-layered model in test 9LuR$^+$, respectively. Each test was carried out under an effective centrifugal acceleration of 100g. The scaling between the model and the prototype was 1/N in the linear dimension and the duration of the bedrock fault movement and 1 for the velocity (Taylor 1995). The basic parameters of these three models before the bedrock fault simulation are summarized in Table 1.

Table 1 Basic parameters of the three centrifuge experiments

Test identity	3LuR	5LuR	9LuR$^+$
Model height after consolidation: mm (prototype in meters)	544 (54.4)	551 (55.1)	557 (55.7)
The distance from surface to the tip of the pre-existing fracture: mm (prototype in meters)	136 (13.6)	138 (13.8)	139 (13.9)
Dipping angle of the pre-existing fracture with respect to the horizontal plane: in degrees	68.7	68.9	69.1

Centrifuge Model Configuration

Figure 2 shows the model box. It was an aluminum plane-strain container fitted with a 100 mm thick Perspex window, which allowed observation of the soil deformation during testing. The internal dimensions of this strong box were 350 mm × 1244 mm × 851 mm (width × length × height).

A test setup was installed in the bottom of the strong box to simulate the bedrock fault system, as shown in Fig. 2(b). The left part of this setup was bolted to the bottom of the strong box to simulate a foot wall. The right part, aiming to simulate a hanging wall, mainly consisted of a hydraulic cylinder and a hanging wall block. Driven by this hydraulic cylinder, the hanging wall block could move along a preset direction at an angle of 70^o with respect to the horizontal plane. This test

setup was designed to model both normal and reverse bedrock fault movements. However, only normal fault movements were considered in this study.

Model Preparation

The sand and silt utilized in this study were both obtained from the Chang Ping area, which is in northern Beijing. Each type of soil was pretreated before being used. The details of the procedures employed were presented in a previous paper (Hu et al. 2009). The soil model was constructed using the moist tamping method. Each compaction layer was about 15 mm high. To reduce the non-homogeneity between the compaction layers, the surface of each compaction layer was scratched before compaction of the following layer. The densities of the sand layer and the silt layer in all tests were fixed at $1.69\times10^{-3}\,\mathrm{g/mm^3}$ and $1.92\times10^{-3}\,\mathrm{g/mm^3}$, respectively. Key soil parameters are summarized in Table 2. Parameter ϕ'_{crit} was obtained from the CU tri-axial test.

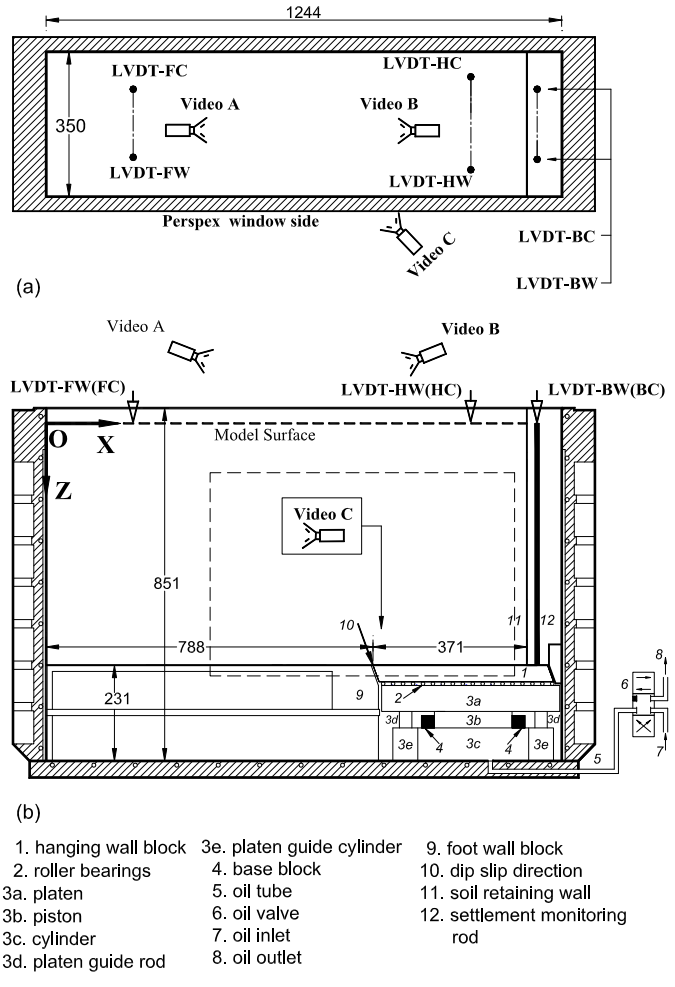

Fig. 2. Model package (dimensions in mm)

During model preparation, a procedure was adopted to embed a filter paper into the soil model to simulate the pre-existing fracture in the soil. The soil models on both sides of the pre-existing fracture were prepared separately. Firstly, the soil model on the footwall was built with the aid of templates. The slope surface designed for the location of pre-existing fracture was exposed to cover a filter paper. This filter paper was used to change the local stress-strain behavior of the soil model. Afterwards, the soil model on the hanging wall was prepared to the height of the pre-existing fracture. Finally, the rest of the soil model was compacted until it reached the target model height.

Table 2 Soil parameters

Soil	D_{50} (mm)	Water content (%)	Plastic Limit (%)	Liquid Limit (%)	ϕ'_{crit} (^{o})
Sand	0.77	5.5	-	-	37
Silt	0.032	20	22	31	33

To demonstrate the effectiveness of the filter paper in pre-existing fracture simulation, two series of direct shear box tests were conducted. The first series of the tests was carried out on natural soil samples. The method of soil preparation was the same as that was adopted in the preparation of the centrifuge model. The tests covered different normal stresses ranging from 100 kPa to 400 kPa. The second series of the tests considered the influence of sandwiched filter paper. During the model compaction, the filter paper with the same cross-sectional area as that of soil sample was sandwiched between the top and bottom halves of the soil sample, as shown in Fig. 3. In this way, the shear failure plane was expected to pass through the plane where the filter paper was located.

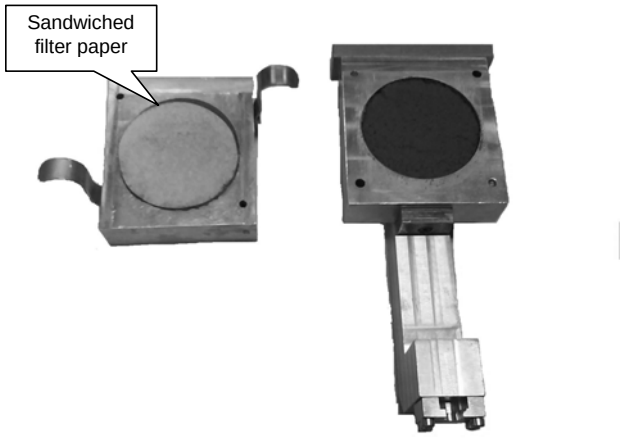

Fig. 3. Sandwiched sample in direct shear box

Figure 4 compares the influence of the embedded filter paper on the stress-strain behavior of the Beijing silt and sand. The identification of the direct shear tests follows the general nomenclature SILT/SAND(F/N)X, where F and N denote tests

with and without filter paper, respectively. X is the normal stress applied to the soil sample.

Figure 4(a) shows the strain hardening behavior of Beijing silt. The shear stress increases gradually until it reaches the ultimate state. The apparent angle of friction at the critical state was approximately 33°. This is consistent with the tri-axial test results, as given in Table 2. When the silt sample was sandwiched with filter paper, no apparent change in the stress-strain behavior was observed.

Figure 4(b) illustrates the post-peak-softening behavior of Beijing sand. The shear strain for reaching the critical state increased gradually as the vertical stress increased. The apparent angle of friction at the critical state for the Beijing sand was found to be 39°, a little larger than that obtained in the tri-axial tests shown in Table 2. By defining the apparent dilation angle as $\psi = \tan^{-1}\left(-\mathrm{d}y/\mathrm{d}x\right)$, it was found that the apparent dilation angle of Beijing sand was about 6°. When sandwiched with filter paper, the apparent dilation angle was reduced to about 3°. At the same time, the "peak" part of the stress strain behavior disappeared on the effect of the filter paper except for the test SAND(F)105.

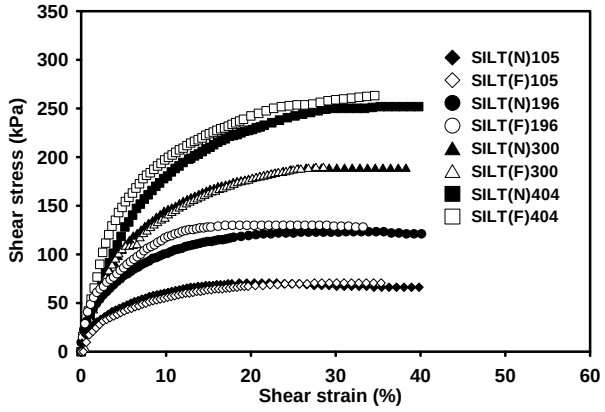

(a) Direct shear tests on silt

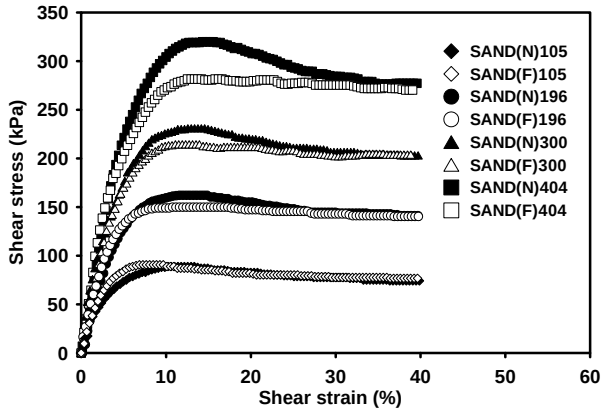

(b) Direct shear test on sand

Fig. 4. Direct shear test results

The reduction of the apparent dilation angle of Beijing sand influenced by the filter paper illustrates that it is reasonable to use the filter paper to change the behavior of the sand surrounding the pre-existing fracture. The effect of the filter paper on the behavior of the Beijing silt may not be that obvious because of its inherent "hardening" behavior.

Instrumentation

After model preparations, the strong box was transferred to the centrifuge. The instrumentation layout for all three tests is shown in Fig. 2(a) and 2(b). Six Linearly Variable Differential Transformers (LVDT), four digital cameras and three digital video recorders were used during the tests. Four of the LVDTs were used to measure the displacement on the model surface and the other two were used to measure the bedrock fault movement. The four digital cameras were mounted in front of the Perspex window to observe model deformation. The observation zone of the four cameras is shown in Fig. 2(b) with the dashed line. The digital images were then analyzed by the Geo-PIV program developed by White et al. (2003). The three digital videos were used to monitor the model surface failure and bedrock fault movement in flight. An assembled model is shown in Fig. 5.

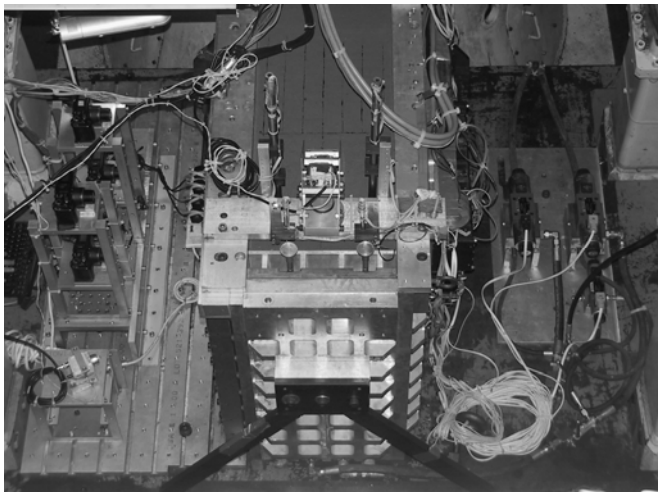

Fig. 5. An assembled centrifuge model

Centrifuge Testing Sequence

The tests commenced with an initial period of consolidation in the centrifuge. It took about 15 minutes to spin up the centrifuge to 100g. This centrifuge acceleration was kept constant during the following 2 hours of consolidation. After consolidation, the normal fault movement was simulated by a downward movement of the hanging wall block. It was controlled by opening oil valve 6 shown in Fig. 2(b). When the oil in the hydraulic cylinder (item 3c in Fig. 2(b)) was drained out, the platen fell down and rested upon the adjustable base block (item 4 in Fig. 2(b)). The vertical settlement of the platen

was guided by four platen guides around the cylinder. After spinning down the centrifuge, the post experiment observations were made and the failure patterns on the model surfaces were recorded.

OBSERVATIONS AND EXPERIMENTAL RESULTS

The experimental results were analyzed to distinguish ground surface failures among different multilayered soils. Data presented here have been converted into prototype measures, unless stated otherwise. The coordinate system adopted for presenting the test result is shown in Fig. 2(b).

Ground Surface Displacement Monitoring Results

Figure 6 shows the typical recorded displacements for each test. Because the model was simplified into a two-dimensional one, settlement results were calculated from the average readings of the LVDTs at the same cross section. For example, the model surface settlement on the foot wall (FootWall-3LuR, FootWall-5LuR, and FootWall-9LuR$^+$) was calculated by averaging LVDT-FC and LVDT-FW. The moment of bedrock fault movement was set as the origin of the ordinate.

In test 3LuR, it can be found that settlement of about 0.44m occurred within 5 s (Bedrock-3LuR), resulting in a velocity of bedrock fault movement of around 0.08 m/s. Simultaneously, the model surface on the hanging wall was displaced at a smaller magnitude of around 0.41 m (HangingWall-3LuR). However, no obvious displacement was observed in the soil model at the foot wall (FootWall-3LuR). A similar trend of displacement results was observed in tests 5LuR and 9LuR$^+$. To compare the influence of the soil profile on the surface differential settlement, all displacement results and the dimensionless ratio of the surface settlement on hanging to the bedrock fault movement are presented in Table 3.

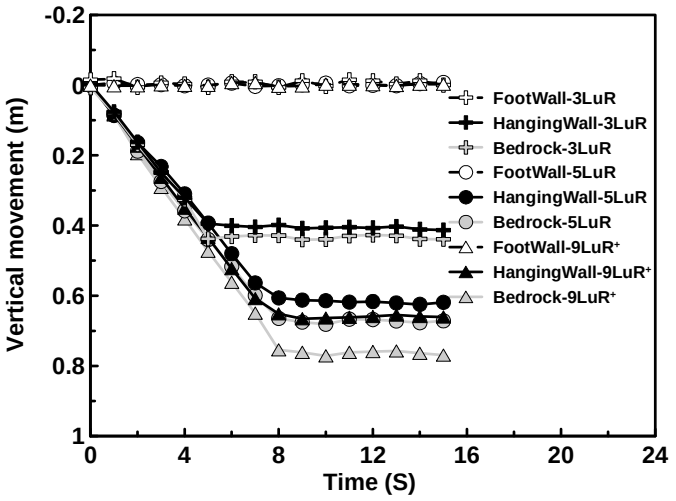

Fig. 6. Vertical movement of ground surface and bedrock

According to the empirical relationships proposed by Wells and Coppersmith (1994), the moment magnitude, M_w, can be expressed as a function of the maximum surface displacement, D (m), $M_w = 6.61 + 0.71 \times \log D$. The moment magnitude corresponding to the bedrock fault movements in tests 3LuR, 5LuR and 9LuR$^+$ were 7.0, 7.2 and 7.2, respectively.

Table 3: Summary of differential settlement on the model surface

Test identity	3LuR	5LuR	9LuR$^+$
Movement of bedrock: m	0.44	0.68	0.76
Surface settlement on foot wall: m	0	0	0
Surface settlement on hanging wall: m	0.41	0.61	0.66
Surface settlement on hanging wall/Vertical movement of bedrock	0.93	0.90	0.87

The displacement results on the model surface show that differential settlement between the foot wall and the hanging wall was triggered by normal fault movements in multilayered soils. This differential settlement on the ground surface appears to be smaller than that in the bedrock fault. Besides, it is interesting to note that the ratio of the surface settlement upon hanging wall to the vertical movement of bedrock fault decreased when the number of soil layers increased. This absorptive tendency of the soil was also observed in field case studies (Bonilla 1970; Bray et al. 1994).

Observed Failure Pattern on the Model Surface

Anastasopoulos et al. (2007) anticipated that $(\mathrm{h/H})_{\mathrm{crit}}$, which is necessary for fault outcropping in normal fault, ranged from 0.75% in dense sand to 1.00% in loose sand. Figure 7 shows the model surface after test 3LuR. No other obvious ground failure can be observed except for the differential settlement in this test. This may be due to the small magnitude of the bedrock fault movement, h, compared to the height of the soil model, H. The value of h/H equaled 0.80% in this test. Since silt has a higher ductility compared to sand under the same stress state, a larger value of $(\mathrm{h/H})_{\mathrm{crit}}$ in three-layered than in dry sand is expected.

Figures 8(a) and 8(b) illustrate the ground surface cracks that were observed in test 5LuR and 9LuR$^+$, respectively. The dashed lines, 1-1', 2-2' and 3-3', drawn in these two figures show the intersections of the bedrock fault plane and the model surface, the projections of the bedrock fault line on the model surface, and the projections of the tip of the pre-existing fracture on the model surface, respectively. They are presented to identify the location of the ground surface cracks.

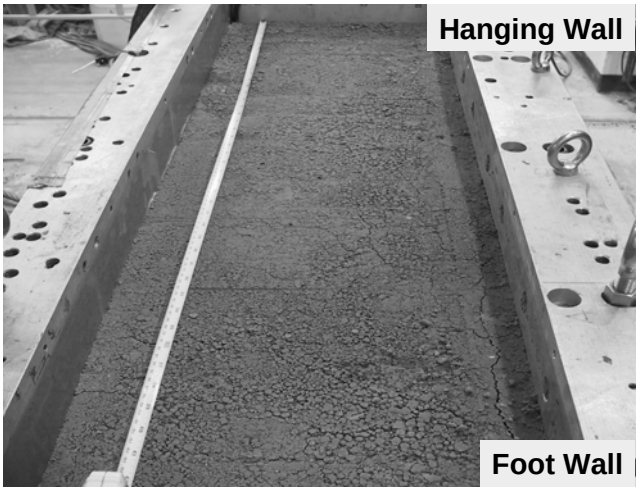

Fig. 7. Ground surface after test in test 3LuR

Figure 8(a) shows that the distance between the two cracks along the center line of the model was about 3.9 m. The maximum width of these cracks was about 0.3 m, with a depth of around 6.9 m. Such a ground failure pattern is quite consistent with that was observed in the silt test and the nine-layered test without considering the pre-existing fracture by Hu et al. (2009).

Figure 8(b) shows the ground surface crack that was observed in test 9LuR$^+$. Only one crack was found in this test even though the bedrock fault movement was larger than in test 5LuR. The distance of this crack to dashed line 1-1' was about 4.8 m along the center line of the model. The maximum width of this crack was about 0.5 m. It passed through the whole top silt layer. In the underlying sand layer, the crack was difficult to identify.

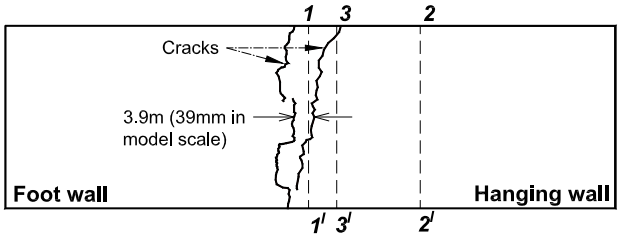

(a) Test 5LuR

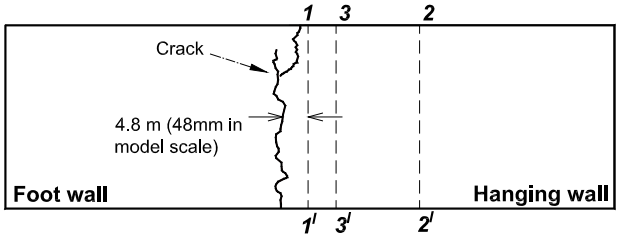

(b) Test 9LuR$^+$

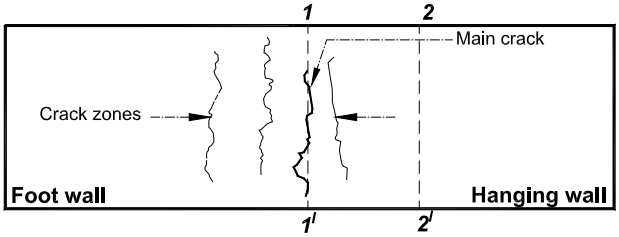

(c) Nine-layered soil with no pre-existing fracture (after Hu et al. 2009)

Fig. 8. Ground surface cracks

Figure 8(c) illustrates the surface cracks that were observed in the nine-layered test reported by Hu et al. (2009). When comparing Fig. 8(b) with Fig. 8(c), it can be found that the pre-existing fracture significantly reduced the width of the cracks on the model surface.

Soil Deformation Patterns

Soil deformations after bedrock fault movement were measured relative to the immediate pre-fault state, using the image processing technique developed by White et al. (2003). Figure 9(a) shows the soil movement that was observed after the bedrock fault movement in test 5LuR. Dashed lines OA and OB were drawn to identify the soil deformation patterns. Both OA and OB passed through the bedrock fault line and tilted at an angle of 70^o with respect to the horizontal plane. With these two lines, the soil deformation can be roughly categorized into three zones. Line OA happens to be the boundary of significant soil movement. In ZONE I, little or no movement can be observed. The soil in ZONE I was unaffected by normal fault movements. Displacement vectors in ZONE II show that the soil in this zone moved in almost the same direction and magnitude. The magnitude of displacement vectors in ZONE III increased from boundary OA to boundary OB.

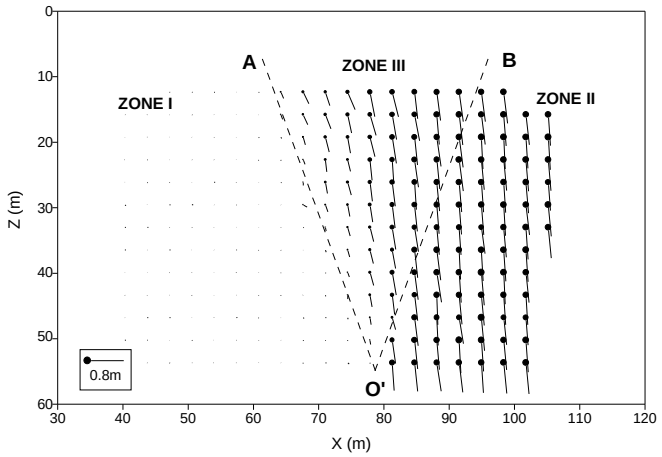

(a) Measured displacement vectors

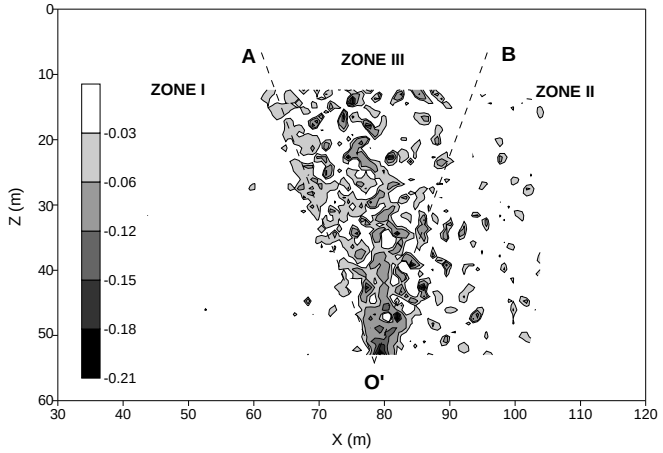

(b) Shear strains in the model ground
Fig. 9. Soil deformation after bedrock fault movement

The shear strain contours, shown in Fig. 9(b), suggests that severe shearing of the soil ground was mainly located in ZONE III. In contrast to the slip surface reported by Nahas et al. (2006) in dry sand, no localized shear band can be found in the five-layered sample when subjected to a normal fault.

CONCLUSIONS

Three centrifuge tests were conducted in this study. The soil ground profiles investigated in these three tests were three-layered, five-layered and nine-layered samples. From the in-flight test monitoring and the post-test observations, the following conclusions are drawn.

Differential settlement on the ground surface tends to be induced by normal fault movements in multilayered soils. This differential settlement occurs simultaneously with the bedrock fault movement. Complex ground profile seems to absorb more bedrock fault movements.

No apparent ground surface crack was observed in the three-layered test when the magnitude of the bedrock fault movement was relatively small (h/H=0.8%). Ground surface cracks were observed in the five-layered and the nine-layered samples after a larger magnitude of bedrock fault movement (h/H=1.2% and h/H=1.4% for test 5LuR and 9LuR$^+$, respectively). Such a failure pattern was also observed in the silt test and the nine-layered sample with no pre-existing fracture. The pre-existing fracture tends to reduce the width of the crack zones on the ground surface during bedrock fault movement.

Digital image analysis shows that the soil deformation in the five-layered sample was roughly divided into three zones: a stationary soil mass in ZONE I, a shearing soil mass in ZONE II, and a downward moving soil mass in ZONE III. No obvious localized shear band was observed in this ground profile when subjected to normal fault movements.

ACKNOWLEDGEMENTS

The authors would like to thank Mr. M. Dong for assisting in preparing for some model tests.

REFERENCES

Ahmed, W., and Bransby, M.F. [2009]. "Interaction of shallow foundations with reverse faults". Journal of Geotechnical and Geoenvironmental Engineering, 135(7), pp. 914-924.

Anastasopoulos, I. [2009]. "Closure to "Fault rupture propagation through sand: Finite-element analysis and validation through centrifuge experiments" by I. Anastasopoulos, G. Gazetas, M. F. Bransby, M. C. R. Davies, and A. El Nahas". Journal of Geotechnical and Geoenvironmental Engineering, 135(6), pp. 846-850.

Anastasopoulos, I., Gazetas, G., Asce, M., Bransby, M.F., Davies, M.C.R., and El Nahas, A. [2007]. "Fault rupture propagation through sand: Finite-element analysis and validation through centrifuge experiments". Journal of Geotechnical and Geoenvironmental Engineering, 133(8), pp. 943-958.

Anastasopoulos, I., Gazetas, G., Bransby, M.F., Davies, M.R., and El Nahas, A. [2009]. "Normal fault rupture interaction with strip foundations". Journal of Geotechnical and Geoenvironmental Engineering, 135(3), pp. 359-370.

Athanasopoulos, G.A. [2009]. "Discussion of "Fault rupture propagation through sand: Finite-element analysis and validation through centrifuge experiments" by I. Anastasopoulos, G. Gazetas, M. F. Bransby, M. C. R. Davies, and A. El Nahas". Journal of Geotechnical and Geoenvironmental Engineering, 135(6), pp. 844-845.

Bonilla, M.G. [1970]. "Surface faulting and related effects" Chapter 3, *Earthquake Engineering*, R.L. Weigel, ed., Prentice Hall, Englewood Cliffs, N. J., pp. 47-74.

Bray, J.D., Seed, R.B., Cluff, L.S., and Seed, H.B. [1994]. "Earthquake fault rupture propagation through soil". Journal of Geotechnical Engineering, 120(3), pp. 543-561.

Cole, D.A., Jr., and Lade, P.V. [1984]. "Influence zones in alluvium over dip-slip faults". Journal of Geotechnical Engineering, 110(5), pp. 599-615.

Faccenna, C., Nalpas, T., Brun, J.P., Davy, P., and Bosi, V. [1995]. "The influence of pre-existing thrust faults on normal fault geometry in nature and in experiments". Journal of Structural Geology, 17(8), pp. 1139-1149.

Hu, P., Cai, Q.P., Luo, G.Y., Ding, Y.H., Dong, M., Hu, L.W., Hou, Y.J., and Ng, C.W.W. [2009]. "Centrifuge modeling of failure patterns in mixed soil layers induced by normal faults". Accepted by the 17th ICSMFE, Egypt, In pressed.

Lade, P.V., Cole Jr, D.A., and Cummings, D. [1984]. "Multiple failure surfaces over dip-slip faults". Journal of Geotechnical Engineering, 110(5), pp. 616-627.

Lazarte, C.A., and Bray, J.D. [1996]. "A study of strike-slip faulting using small-scale models". Geotechnical Testing Journal, 19(2), pp. 118-129.

Nahas, A.E., Bransby, M.F., and Davies, M.C.R. [2006]. "Interaction between normal fault rupture and rigid strong raft". *Proceeding of International Conference on Physical Modelling in Geotechnics*, Hong Kong, pp. 337-342.

Ng, C.W.W., Li, X.S., Van Laak, P.A., and Hou, D.Y.J. [2004]. "Centrifuge modeling of loose fill embankment subjected to uni-axial and bi-axial earthquakes". Soil Dynamics and Earthquake Engineering, 24(4), pp. 305-318.

Ng, C.W.W., Van Laak, P.A., Tang, W.H., Li, X.S., and Zhang, L.M. [2001]. "The Hong Kong Geotechnical Centrifuge". *Proceedings of the Third International Conference on Soft Soil Engineering*, pp. 225-230.

Taylor, R.N. [1995], "Centrifuges in modelling: Principles and scale effects" Chapter 2, Geotechnical Centrifuge Technology, R.N. Taylor, ed., Blackie Academic & Professional, London, pp. 19-33.

Wells, D.L., and Coppersmith, K.J. [1994]. "New empirical relationships among magnitude, rupture length, rupture width, rupture area, and surface displacement". Bulletin of the Seismological Society of America, 84(4), pp. 974-1002.

White, D.J., Take, W.A., and Bolton, M.D. [2003]. "Soil deformation measurement using particle image velocimetry (PIV) and photogrammetry". Geotechnique, 53(7), pp. 619-631.